nature communications

Article

https://doi.org/10.1038/s41467-024-54794-x

Cullin-5 deficiency promotes chimeric antigen receptor T cell effector functions potentially via the modulation of JAK/STAT signaling pathway

Received: 23 March 2023

Accepted: 21 November 2024

Published online: 10 December 2024

Check for updates

Yoshitaka Adachi[1] ✉, Seitaro Terakura[1] ✉, Masahide Osaki[1], Yusuke Okuno[2], Yoshitaka Sato[3], Ken Sagou[1,3], Yuki Takeuchi[1], Hirofumi Yokota[1], Kanae Imai[1], Peter Steinberger[4], Judith Leitner[4], Ryo Hanajiri[1], Makoto Murata[1] & Hitoshi Kiyoi[1]

Chimeric antigen receptor (CAR) T cell is a promising therapy for cancer, but factors that enhance the efficacy of CAR T cell remain elusive. Here we perform a genome-wide CRISPR screening to probe genes that regulate the proliferation and survival of CAR T cells following repetitive antigen stimulations. We find that genetic ablation of *CUL5*, encoding a core element of the multi-protein E3 ubiquitin-protein ligase complex, cullin-RING ligase 5, enhances human CD19 CAR T cell expansion potential and effector functions, potentially via the Janus kinase/signal transducers and activators of transcription (JAK/STAT) pathway. In this regard, CUL5 knockout CD19 CAR T cells show sustained STAT3 and STAT5 phosphorylation, as well as delayed phosphorylation and degradation of JAK1 and JAK3. In vivo, shRNA-mediated knockdown of CUL5 enhances CD19 CAR T treatment outcomes in tumor-bearing mice. Our findings thus imply that targeting CUL5 in the ubiquitin system may enhance CAR T cell effector functions to enhance immunotherapy efficacy.

Adoptive T cell therapy with gene-modified T cells expressing chimeric antigen receptor (CAR) has shown promising clinical outcomes, specifically in B-cell hematologic malignancies[1–4]. Numerous research has found that in vivo expansion and long-term persistence of CAR T cells are hallmarks of treatment success following CD19 CAR T cell therapy[5–7]. To boost CAR T cell persistence, several types of CAR T cells have been developed, such as those with modified immunoreceptor tyrosine-based activation motifs or modified costimulatory domains[8–10]. Moreover, one of the promising techniques for enhancing CAR T cell persistence is to modify specific genes that regulate T cell function. It has been reported that improving specific gene expression[7,11], epigenetic regulation of all human genes[12], or genetic ablation using the clustered regularly interspaced short palindromic repeats (CRISPR) and CRISPR-associated protein 9 (CRISPR-Cas9) procedure can improve T cell memory and in vivo persistence[13,14]. This strategy could be applied not only to CAR T cell therapy but also to other adoptive cell therapies, and help achieving a better comprehension of the kinetics of antigen-specific T cell in general.

Genome-wide pooled (GW) CRISPR screening has recently emerged as a powerful tool for conducting large-scale loss-of-function screens on human primary immune cells[15–18]. It can be applied to primary human T cells by a combination of a pooled lentiviral guide RNA

[1]Department of Hematology and Oncology, Nagoya University Graduate School of Medicine, Nagoya, Japan. [2]Department of Virology, Nagoya City University Graduate School of Medical Sciences, Nagoya, Japan. [3]Department of Virology, Nagoya University Graduate School of Medicine, Nagoya, Japan. [4]Division for Immune Receptors and T Cell Activation, Institute of Immunology, Medical University of Vienna, Vienna, Austria. ✉e-mail: yadachi@umich.edu; tseit@med.nagoya-u.ac.jp

(gRNA) transduction and electroporation of the Cas9 protein. In CRISPR screening for primary T cells or CAR T cells, specific gene libraries, including transcription factor genes or genes related to epigenetics, have typically been used as pooled libraries, and novel study findings using GW CRISPR library screening in human CAR T cells have been published, and have revealed molecules that affect T cell traits, and genetic mutations that confer resistance to T cell immunotherapy[18–20]. Given that T cell function is regulated in a variety of ways, it may be plausible to enhance CAR T-cell proliferation via previously-unknown mechanisms.

We hypothesized that developing an in vitro human CD19 CAR T cell model that uses prolonged intermittent antigen stimulation for GW CRISPR screening would reveal new insights into CAR T cell proliferation. In contrast to the in vivo screening model using mouse T cells[21,22], the in vitro human CAR T cell model enables scalability, ease of manipulation, and the possibility of determining genes that cannot be detected in mouse T cell screening[23].

In this study, we use GW CRISPR-Cas9 knockout (KO) screening in human CAR T cells to reveal specific candidate genes that can control CAR T cell proliferation and survival. We find that cullin-RING ligase 5 (Cullin-5, CUL5), encoding a core element of the multi-protein E3 ubiquitin-protein ligase complex, which is involved in regulating T cell proliferation potentially via the Janus kinase/signal transducer and activator of transcription (JAK/STAT) signaling pathway. Furthermore, we validate the effect of CUL5 KO or CUL5 knockdown (KD) in the context of CAR T cell therapy using immunocompromised mice model. The modification of CUL5 with short hairpin RNA (shRNA) allows for safer and simpler CUL5 KD, which may have broad applicability in a variety of T cell-based therapies.

Results

GW CRISPR screening identifies candidate proliferation regulator genes

The GW CRISPR gRNA library-encoding lentiviral system (Genome-scale CRISPR Knock-out lentiviral pooled library Version 2, GeCKOv2) was adopted to identify candidate genes that regulate CAR T cell effector function[24]. To verify the KO efficiency and develop an optimized approach for simultaneous GW KO and CD19 CAR transduction, first we knocked out CD8 and then transduced CD19 CAR to determine the experimental conditions. When CD8 single gRNA (sgRNA) was successfully transduced, green fluorescent protein (GFP) was expressed. In the optimized approach, ~70% KO efficiency with 40%–50% CD19 CAR positivity was obtained before CAR purification (Fig. 1a and Supplementary Fig. 1a), implying that GW CRISPR screening can be applied to primary CD19 CAR T cells. After a purification by CAR-transduction marker (truncated EGFR) on day 7, CAR positive cells were >95% and GFP positive cells were ~70%. When the GeCKOv2 library-encoding lentivirus was applied to create GW CRISPR KO-CD19 CAR T cells, 91%–99% of gRNA was detected on Day 10 before the first CD19 stimulation (Supplementary Fig. 1b). Following repetitive stimulation, surviving CD19 CAR T cells were collected, genomic DNA (gDNA) was extracted, and gRNA sequences were identified. When we examined the skewness ratio after and during repetitive stimulation, the distribution of reads per guide continued to skew until day 40[25] (Supplementary Fig. 1c). In this study, the GFOLD analysis procedure was used, where GFOLD greater than 2 is generally correlated with a change of about $\log_2$ fold change (FC) greater than 2[26]. GFOLD is a software that calculates conservative fold change from NGS count data. It calculates GFOLD values, which are conservative estimations of fold changes between two groups. If the values of a gene did not show a statistically significant difference with a provided p-value threshold, the GFOLD value is 0. Otherwise GFOLD values roughly correlate with raw fold changes. A greater fold change of a guide between Day 10 and Day 40 indicates T cells having the guide increased the proportion in the culture. This can be caused by better proliferation or survival caused by the knockout of the gene targeted by the guide. GFOLD analysis suggested that there were 2299, 2102, and 2030 gRNA with GFOLD greater than 2 in each donor's CD19 CAR T cells. The highest score was then assigned from the top of the GFOLD rank, so the top-ranked genes received scores of 2299, 2102, and 2030, while the lowest-ranked genes received a score of 1 (Fig. 1b). Guides with GFOLD < 2 were given the score of 0. Then the score of each gene obtained from each donor was summed (Fig. 1c). Based on the findings of Q value, GFOLD evaluation, and gene expression in T cells, six candidate genes (*SMCO2*, *TSR2*, *PKM*, *CUL5*, *KLRC1*, and *ING3*) were selected.

To further narrow down the candidates, validation experiments were performed by knocking out individual genes using the same technique as the GW screening. Two distinct sgRNAs were applied for each gene to create gene KO-CD19 CAR T cells. Each plasmid encoding a sgRNA designed to express GFP when transduced. GFP were ~40%–50% positive after a transduction culture. When GFP expression was monitored during the culture period, only CUL5 KO-CD19 CAR T cells showed an increase in the GFP+ fraction (Fig. 1d). In addition, western blotting analysis revealed that CUL5 expression was lowered to about 20%–30% in CUL5 KO-CD19 CAR T cells (Fig. 1e, f). Furthermore, GFP percentages significantly increased upon repetitive CD19 stimulations (Fig. 1g). Next, we performed experiments using our CD37-targeting CAR to determine whether the same results would be obtained in combination with other CAR[27]. Again we observed that GFP percentages significantly increased in CUL5 KO-CD37 CAR T cells upon repetitive antigen (Ag) stimulations (Fig. 1h). Therefore, a candidate gene, *CUL5*, which affects the regulation of CAR T cells, was successfully selected via repetitive Ag stimulation experiments. Moreover, these findings imply that CUL5 KO could improve the expansion potential of two types of CAR T cells in response to Ag stimulation.

CUL5 KO enhances CD19 CAR T-cell proliferation and effector functions in vitro

To identify changes in CUL5 KO-CD19 CAR T cells, detailed alterations in GFP positivity were first investigated over time. In two distinguished sgRNA-modified CAR T cells, GFP percentages increased later in culture (Fig. 2a–d). Additionally, to validate the mechanism by which CUL5 sgRNA+ fraction has a greater ability for expansion than sgRNA− fraction, several proliferation assays were performed. CellTrace Violet (CTV) division analysis indicated an accelerated cell division only within the GFP+ fraction, notably on Days 4–7 of culture (Fig. 2e–g). In addition, the percentages of Ki67+ (Fig. 2h, i) and EdU+ cells (Supplementary Fig. 2a and b) in CUL5 KO-CD19 CAR T cells were significantly greater only in the later time course. However, the percentage of apoptotic cells in control CD19 CAR T cells and CUL5 KO-CD19 CAR T cells upon Ag stimulation were comparable (Supplementary Fig. 2c). These findings indicate that CUL5 KO boosted cell division in activated CAR T cells but did not inhibit apoptosis. In addition, cytokine secretion capacity was significantly higher in CUL5 KO-CD19 CAR T cells stimulated with CD19+ Raji cells, whereas cytokine was not secreted upon CD19- K562 stimulation (Fig. 2j–l). To examine changes in CD25 (IL-2 receptor alpha) expression after Ag stimulation, CAR T cells and γ-irradiated Raji cells were mixed at a 1:1 ratio and cultured under IL-2 addition. CD25 expression was significantly higher in CUL5 KO-CD19CAR T cells than in control KO-CD19CAR T cells (Fig. 2m, day 4 – 7; Supplementary Fig. 2d). Moreover, to examine the effect of CUL5 KO on the T cell phenotype after stimulation, we used two different stimulation methods: CD3/CD28 beads stimulation mimicking T cell receptor (TCR) stimulation and CD19CAR-mediated stimulation by Raji cells. CUL5 KO-CD19 CAR T cells showed higher effector memory (CD45RA (−)-C-C chemokine receptor 7 (CCR7 −)) and lower central memory (CD45RA (−)-CCR7 (+)) phenotypes after stimulation with both CD3/CD28 beads (Fig. 2m, n, and p) and irradiated Raji cells (Fig. 2m, o, and q) than control CD19

https://doi.org/10.1038/s41467-024-54794-x

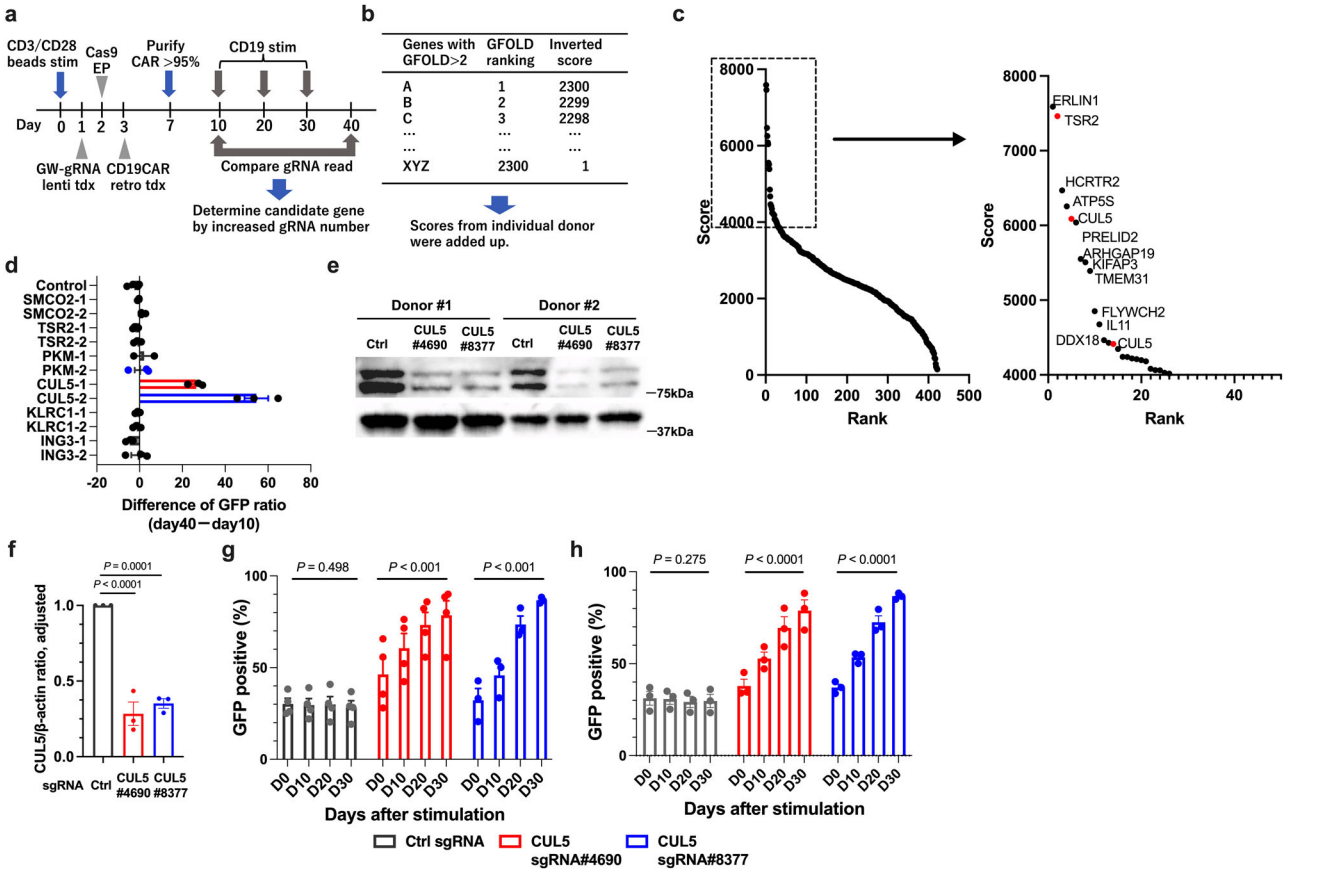

Fig. 1 | Genome-wide clustered regularly interspaced short palindromic repeats (GW CRISPR) knockout (KO) screening of CD19 chimeric antigen receptor (CAR) T cells identified CUL5 as a candidate gene to enhance CAR T-cell survival. a Outlines of the GW CRISPR KO screening of CD19 CAR T cells. After Day 10 of the culture, GW CRISPR KO-CD19 CAR T cells were repeatedly stimulated with γ-irradiated Raji cells. DNAs from CAR T cells at Days 10 and 40 were compared using next-generation sequencing. Stim, stimulation; EP, electroporation; tdx, transduction. **b** GFOLD score data and calculation. Genes with GFOLD greater than 2 were ranked. Individual ranking scores were added up from top to bottom ($n = 3$). **c** GFOLD score summary of three replicated data from three donors. The right panel depicts the expansion of the dotted area. **d** Secondary CRISPR KO screening of CD19 CAR T cells. Each of the six candidate genes was knocked out using two different sgRNAs. Data from experiments on three different donors are acquired and presented as the mean and standard error of the mean. **e**, **f** CUL5 KO using two different sgRNAs and its efficiency. The immunoblots show CUL5 expression in sgRNA-transduced CD19 CAR T cells (**e**). CUL5 to β-actin expression ratio in sgRNA-transduced CD19 CAR T cells (**f**). ($n = 3$, different donors) (**g**, **h**) Green fluorescent protein (GFP) positivity in different types of CUL5 KO-CAR T cells over time. CD19 CAR T cells (**g**) and CD37 CAR T cells (**h**) were stimulated by γ-irradiated tumor cells. Raji cells were used for Ag stimulation in both CD19 and CD37 CAR T cells. GFP-positive cells were sgRNA-transduced cells. ($n = 4$ for Ctrl sgRNA and CUL5 sgRNA#4690, $n = 3$ for CUL5 sgRNA#8377, different donors in **g**, $n = 3$, different donors in (**h**) Data were expressed as mean ± SEM. One-way ANOVA was used for comparing Ctrl and sgCUL5 (**f**). Two-way ANOVA with Tukey's multiple comparisons test (with adjustment) was used for (**g** and **h**). Source data are provided as a Source Data file.

CAR T cells. Furthermore, CCR7 expression was significantly lower in CUL5 KO-CD19 CAR T cells (Fig. 2r). Still, CUL5 KO did not elevate the expression of exhaustion markers, even following repeated stimulation (Supplementary Fig. 2e). After a short culture time, cytotoxicity in CUL5 KO-CD19 CAR T cells was comparable to control CD19 CAR T cells (Supplementary Fig. 2f). Hence, these findings imply that CUL5 KO improves not only proliferation but also the effector roles of CAR T cells.

CUL5 KO enhances the Janus kinase/signal transducers and activators of the transcription (JAK/STAT) pathway in CAR T cells

To further examine the impacts of CUL5 KO, RNA-Seq analysis was performed on control sgRNA-modified CAR T cells as well as two distinct CUL5 sgRNA-modified CAR T cells. When comparing sgRNA#4690-modified and sgRNA#8377-modified CAR T cells, no differentially expressed genes (DEGs) were detected ($q < 0.01$). In contrast, 51 and 54 DEGs were identified in sgRNA#8377 and sgRNA#4690 CUL5 KO-CAR T cells, respectively, when compared to control sgRNA-modified CAR T cells (Fig. 3a). Additionally, 26 of the 79 DEGs identified by the comparisons between control sgRNA-modified CAR T cells and CUL5 sgRNA-modified CAR T cells were overlapped, implying that CUL5 KO-CD19 CAR T cells modified by two diverse sgRNAs had similar profiles (Fig. 3b). Furthermore, there were many cytokine-related genes in upregulated DEGs by CUL5 KO, implying that CUL5 may be a negative regulator of inflammatory response via cytokine signaling in CAR T cells (Fig. 3c). Over-representation examination revealed enrichment of upregulated genes in interleukin (IL)−2/STAT5 signaling, apoptosis, IL6/JAK/STAT signaling, and the inflammatory response (Fig. 3d). Therefore, these findings corroborate the hypothesis that CUL5 regulates CAR T-cell effector functions primarily via the JAK/STAT pathway.

CUL5 KO enhances STAT3 and STAT5 phosphorylation via IL-2 cytokine signaling in CAR T cells

CUL5 is a core component of cullin-RING ligase 5 (CRL5), a multi-protein E3 ubiquitin-protein ligase complex[28]. The CRL5 complex mediates target protein ubiquitination and proteasomal degradation. The target specificity is determined by the variable substrate recognition component, including a substrate receptor protein called a

https://doi.org/10.1038/s41467-024-54794-x

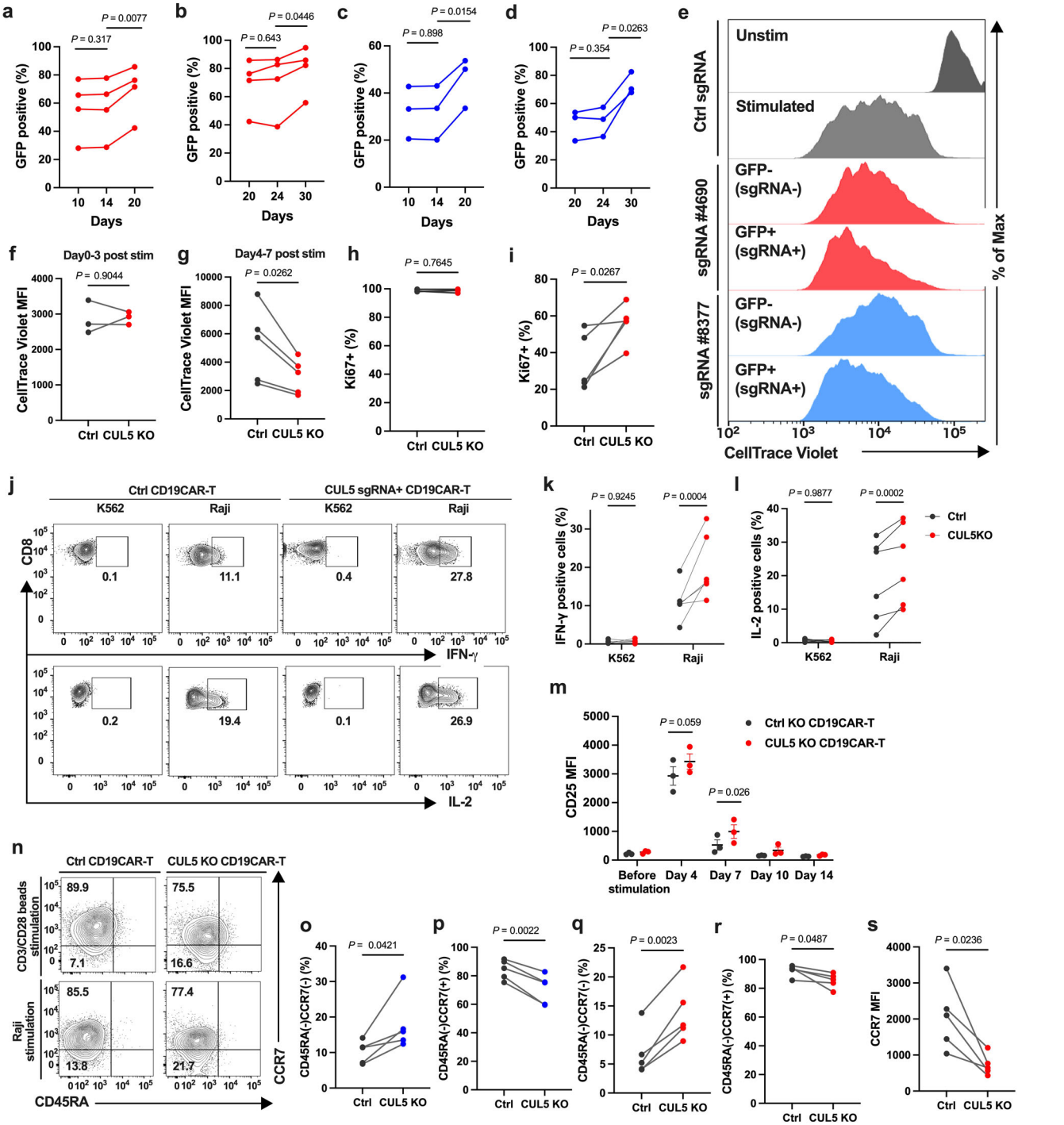

Fig. 2 | CUL5 knockout (KO) promotes sustained proliferation and enhances effector functions later after stimulation. a–d Changes in the percentage of CUL5 KO-CD19 CAR T cells generated by sgRNA#4690 from Days 10–20 (**a**) and 20–30 (**b**) or by sgRNA#8377 from Days 10–20 (**c**) and 20–30 (**d**). ($n = 4$ in **a** and **b**; $n = 3$ in c and **d**) (**e**) Representative flow plots of CellTrace Violet (CTV)-labeled control (Ctrl) or CUL5 KO-CD19 CAR T-cell division assays. GFP− fractions are unmodified CAR T cells, whereas GFP+ fractions are CUL5 KO-CAR T cells. **f**, **g** CTV mean fluorescence intensity (MFI) after stimulation at either earlier (**f**, Days 0–3, $n = 3$) or later time points (**g**, Days 4–7, $n = 5$) in Ctrl or CUL5 KO-CD19 CAR T cells. **h**, **i** Ki-67+ cell percentage after stimulation during earlier (**h**, Days 0–3, $n = 4$) or later (**i**, Days 4–7, $n = 5$) culture periods in Ctrl or CUL5 KO-CD19 CAR T cells. **j** Intracellular cytokine staining of Ctrl or CUL5 KO-CD19 CAR T cells stimulated with K562 or Raji cells. Representative flow plots of interferon-gamma (IFN-γ) and interleukin (IL)-2 are shown. **k**, **l** Intracellular cytokine staining for IFN-γ (**k**) and IL-2 (**l**). ($n = 5$) (**m**) CD25 MFI after Raji stimulation in Ctrl or CUL5 KO-CD19CAR T cells. Data were expressed as mean ± SEM. ($n = 3$) (**n**) Phenotype analysis of Ctrl and CUL5 KO-CD19 CAR T cells for CD45RA and C-C chemokine receptor 7 (CCR7) on Day 30. **o**, **p** Percentages of CD45RA(−)-CCR7(−) effector memory T cells and CD45RA(−)-CCR7(+) central memory T cells after CD3/CD28 beads stimulation. **q, r** Percentages of CD45RA(−)-CCR(−) effector memory T cells and CD45RA(−)-CCR7(+) central memory T cells after Raji cell stimulation. **s** CCR7 MFI after Raji stimulation. ($n = 5$ in (**o**–**s**) Data from three to five different donors are acquired and each dot represents data from each donor. The paired two-sided Student's *t*-test was used for (**a**–**d, f**–**i**, and **o**–**s**). The two-way ANOVA with the Šidák multiple comparisons test was used for (**k** and **l**). The multiple unpaired *t*-test was used for (**m**). Source data are provided as a Source Data file.

https://doi.org/10.1038/s41467-024-54794-x

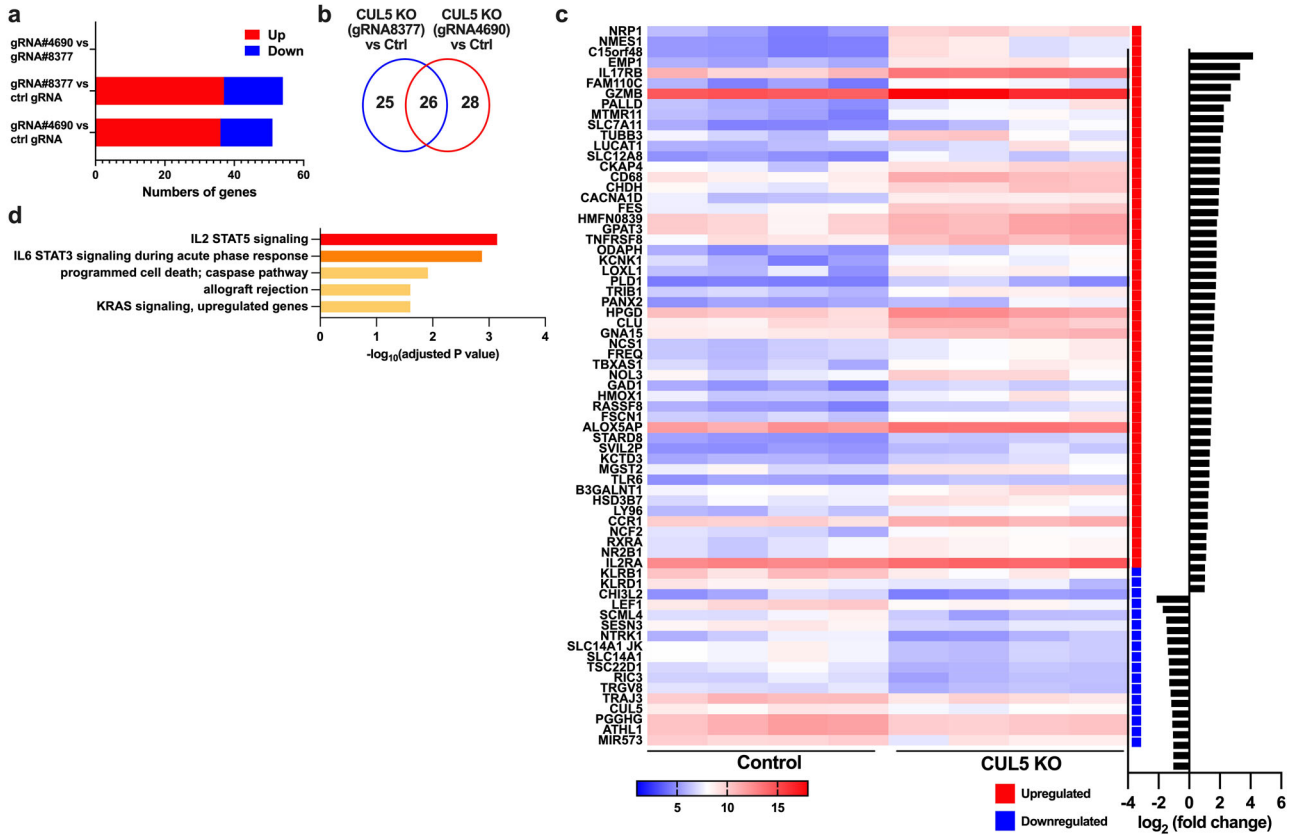

Fig. 3 | CUL5 knockout (KO) CD19 chimeric antigen receptor (CAR) T cells upregulate the Janus kinase/signal transducers and activators of the transcription (JAK/STAT) pathway. a Numbers of differentially expressed genes (DEGs) in control (Ctrl) and two different sgRNA-modified CUL5 KO-CD19 CAR T cells (Ctrl: $n = 4$, sgRNA#4690: $n = 4$, and sgRNA#8377: $n = 3$). **b** Venn diagram of DEGs in CUL5 KO-CD19 CAR T cells prepared using two different sgRNAs. **c** Heatmap displaying the significantly upregulated and downregulated genes in comparisons between CUL5KO-CD19CAR T cells treated with sgRNA#4690 and Ctrl CAR T cells. Each column represents the respective donor's result. **d** Over-representation analysis (hallmark gene sets) of upregulated genes in CUL5 KO-CD19 CAR T cells versus Ctrl sgRNA-transduced CD19 CAR T cells. The *p*-values were all adjusted by Benjamini–Hochberg false discovery rate (FDR) procedure. $-\log_{10}$ (adjusted *p*-value) is shown.

suppressor of cytokine signaling (SOCS). SOCS proteins are cytokine signaling inhibitors and are considered to function as substrate receptors in the ubiquitin system[29,30]. CUL5 acts as a scaffold protein for the CRL5 E3 ubiquitin ligase complex[28,31]. Within the CRL5 complex, SOCS proteins selectively bind to substrates, bringing the substrate and E2 ubiquitin ligase into proximity to ubiquitinate them. Hence, SOCS proteins partake in substrate selection, whereas CUL5 serves as a scaffold protein for their binding. Accordingly, CUL5 KO is assumed to have the same effect as knocking out numerous SOCS family proteins simultaneously. Hence, we hypothesized that CUL5 KO elevates the proliferation of stimulated CD19 CAR T cells by delaying the degradation of target proteins or phosphoproteins.

Based on the RNA-Seq analysis findings and its functions as a CRL5 core component, we hypothesized that CUL5 KO enhances the phosphorylation of proteins in the JAK/STAT pathway. CAR T cells were cultured in vitro with IL-2 supplementation, which is required for T cell survival. Besides IL-2 signaling, in terms of regulation of common γ-chain family receptor signaling, JAK1 and JAK3 are phosphorylated in the downstream, and STAT3 and STAT5 are phosphorylated further downstream of the pathway[32]. Accordingly, we further investigated JAK1/JAK3 signaling and STAT3/STAT5 signaling after CUL5 KO. STAT proteins located downstream of the IL-2 receptor are majorly STAT3 and STAT5[33], and their signaling was also improved in CUL5 KO-CD19 CAR T cells in our RNA-Seq analysis. Therefore, intracellular phosphoflow examination of phospho-STAT3 (p-STAT3) and p-STAT5 was performed with Ag stimulation. The investigation showed that CUL5 KO increased p-STAT3 (Fig. 4a, b) and p-STAT5 (Fig. 4c, d) in CUL5 KO-CD19 CAR T cells. In addition, p-STAT5 expression loss was delayed in CUL5 KO-CD19 CAR T cells after Ag stimulation without IL-2 supplementation (Fig. 4e). We observed prolonged p-STAT3 and p-STAT5 signaling in CUL5 KO CAR T cells, however, the effect was stronger in p-STAT3 than p-STAT5.

Optimal T-cell activation and proliferation necessitate three distinct signals, such as T cell receptor engagement, co-stimulation, and cytokine engagement[34]. Our CD19 CAR construct has a CD3ζ domain as a mimic of TCR signal[3]. Thus, we investigated whether CUL5 KO enhanced the TCR signal to know the pathway where CUL5 participated. Nuclear factor-kappa B, AP-1, and nuclear factor of activated T cell signals, which are representative downstream of TCR signals, were assessed using Jurkat TPR cells[35,36]; nevertheless, CUL5 KO did not boost these signals when stimulated with CD19 Ag (Supplementary Fig. 3a). Moreover, intracellular phosphoflow analysis was used to assess p-ERK and p-p38 signals in CUL5 KO-CD19 CAR T cells and revealed comparable intensities in control CD19 CAR T cells and CUL5 KO-CD19 CAR T cells (Supplementary Fig. 3b). Hence, these findings imply that CUL5 enhances downstream of cytokine signals such as p-STAT3 and p-STAT5 via IL-2 stimulation, not those of TCR signals.

CUL5 downregulation increases p-JAK1/3 expression only in activated CAR T cells

CUL5 is a scaffold protein that is a component of the ubiquitin E3 ligase[28,31]. Some adapter proteins can bind to substrates such as the JAK family and degrade target substrate proteins[30]. Still, the mechanisms by which CUL5 downregulation could influence the dynamics of the

https://doi.org/10.1038/s41467-024-54794-x

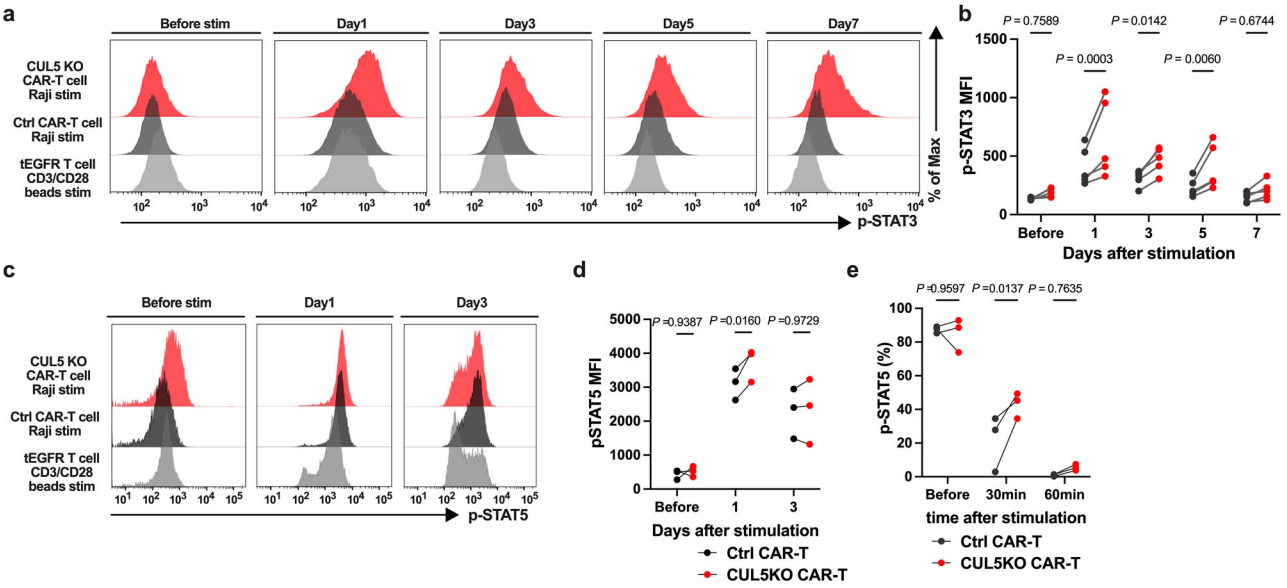

Fig. 4 | CUL5-knockout (KO) CD19 chimeric antigen receptor (CAR) T cells demonstrate intracellular signaling augmentation via phospho-STAT3 (p-STAT3) and p-STAT5. a, **c** Representative flow plots of intracellular p-STAT3 (**a**) and p-STAT5 (**c**). Truncated epidermal growth factor receptor (tEGFR)-transduced T cells were stimulated with anti-CD3/CD28 beads, whereas control (Ctrl) and CUL5 KO-CD19 CAR T cells were stimulated with Raji cells in a 1:5 ratio. The data represent five and three independent experiments on different donors, respectively in (**a** and **c**). **b** The mean fluorescence intensity (MFI) of p-STAT3 at the indicated time after stimulation. ($n = 5$, different donors) (**d**) The MFI of p-STAT5 at the indicated time after stimulation. ($n = 3$, different donors) (**e**) p-STAT5+ percentage at the indicated time after stimulation with Raji cells in medium without interleukin (IL)-2 supplementation. ($n = 3$, different donors) Each dot represents data from each donor. Note that the two-way ANOVA with the Šidák multiple comparisons test was used for (**b**, **d**, and **e**). Source data are provided as a Source Data file.

JAK family in primary CD8 + T cells or CAR T cells have yet to be reported. Hence, we concentrated on the JAK family to assess their expression and phosphorylation. In the inactive state, CUL5 KO did not affect the JAK family, STAT3, or STAT5 expression (Supplementary Fig. 4a). Nevertheless, p-JAK3 expression was reduced in non-activated CUL5 KO-CD19 CAR T cells (Supplementary Fig. 4b).

Manufacturing specific gene KO-CAR T cells requires electroporation, making it challenging to prepare a large quantity of CAR T cells. Thus, to acquire a large number of CUL5-downregulated CAR T cells, clinically applicable CUL5 KD-CD19 CAR T cells were developed, which can be manufactured via only one lentiviral transduction process. A lentivirus vector with shRNA targeting GFP or CUL5 and a CD19 CAR with a truncated epidermal growth factor receptor (tEGFR) linked in a series was first developed (Fig. 5a). The GFP+ Jurkat cells were then transduced with this lentivirus vector, and GFP expression intensity was reduced in the tEGFR-positive fraction (Supplementary Fig. 4c). Following that, SUP-T1 cells were transduced with a lentivirus vector carrying shCUL5 and a CD19 CAR with tEGFR. According to western blotting analysis, CUL5 expression was remarkably lowered in CUL5 KD-CD19 CAR-transduced SUP-T1 cells (Supplementary Fig. 4d and e). Likewise, CUL5 expression was lowered in CUL5 KD-CD19 CAR T cells transduced with a lentiviral two-in-one vector carrying shCUL5 (Fig. 5b and c). In the active state under Ag simulation, CUL5 KD enhanced p-JAK1, p-JAK3, and native JAK3 expressions (Fig. 5d–f). To identify whether this occurs via IL−2 signaling, the expression of JAKs downstream of the IL−2 receptor was assessed in KHYG-1 cells, which are IL−2-dependent cell lines similar to primary CD8 + T cells. CUL5 KD was found to improve JAK1, p-JAK1, JAK3, and p-JAK3 expression (Fig. 5g). Nevertheless, JAK3 expression was only enhanced in response to IL−2 stimulation (Fig. 5g), which is similar to that in CUL5 KD-CD19 CAR T cells. Remarkably, JAK loss was delayed in CUL5 KD-KHYG-1 cells when activated simultaneously with IL-2 and cycloheximide, which hinders the translocation phase in protein synthesis (Fig. 5h). These findings suggest that CUL5 functions in JAK degradation and is responsible for JAK3 degradation via IL-2 signaling-mediated activation. To examine whether substrate receptor KO, rather than CUL5 KO, have the same effect, we selected substrate receptors that have been reported to bind to JAK family protein[28], and further included CISH, which is known to improve NK cell function by ablation[37]. SOCS1, SOCS3, and ASB2 have been identified as typical adapter proteins that degrade JAKs as a substrate and bind CUL5[30]. Hence, we investigated whether knockouts of these genes could trigger the same phenomenon as CUL5 KO. For SOCS1, SOCS3, and ASB2, we confirmed a good level of KO efficiency, but could not confirm CISH KO efficiency in SUP-T1 cells due to low expression of CISH in control SUP-T1 cells (Supplementary Fig. 4f and g). We further performed CISH KO experiments with NK-92 cell line and confirmed that the KO efficiency of CISH was comparable with others (Supplementary Fig. 4g). SOCS1, ASB2, and CISH KO were found to induce much weaker impact on T cell expansion than CUL5 KO (Fig. 5i). These findings corroborate the hypothesis that the proliferation potential of CUL5 KO-CD19 CAR T cells may be owing to the cumulative impact of multiple adapter protein dysfunctions provided that CUL5 is the redundant scaffold protein that binds multiple adapter proteins.

Antitumor activity and development of clinically relevant CUL5 KD-CD19 CAR T cells

In this study, the antitumor potency of CUL5 KO-CD19 CAR T cells was investigated in vivo. NOD-Shi-scid IL-2Rγ KO (NOG) mice were treated with 1×10^6 CAR T cells on Day 7 after being injected with 5×10^5 Raji cells transduced with a construct expressing a GFP-firefly luciferase fusion protein (Raji-ffluc cells; Fig. 6a). CUL5 KO-CD19 CAR T cells inhibit tumor progression more efficiently than control CD19 CAR T cells (Fig. 6b and c), resulting in considerably longer overall survival of CUL5 KO-CD19 CAR T cell-treated mice (Fig. 6d).

As previously stated, CUL5 KD-CD19 CAR T cells were developed and regarded as clinically applicable because of their ease of establishment. On Day 7 following CD8 + T cell isolation, nearly 30-fold more CUL5 KD-CD19 CAR T cells were generated than CUL5 KO-CD19 CAR T cells (Fig. 6e). In addition, the proliferation potential of CUL5

https://doi.org/10.1038/s41467-024-54794-x

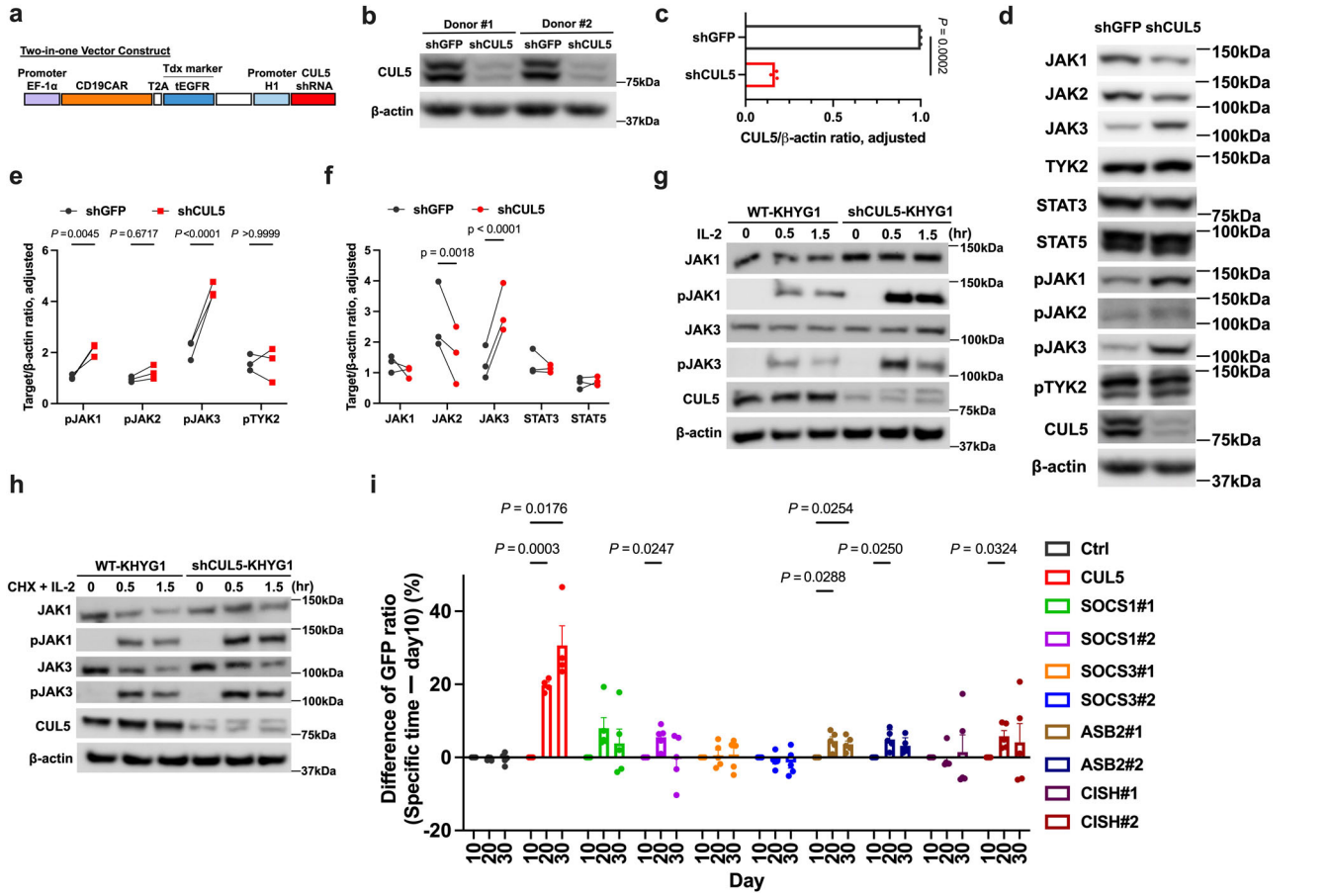

Fig. 5 | CUL5 is involved in Janus kinase 3 (JAK3) degradation in response to interleukin (IL)-2 signaling-mediated activation. a A two-in-one lentiviral vector construct in which CUL5 shRNA and CD19 chimeric antigen receptor (CAR) are linked. **b** The efficiency of CUL5 knockout (KO) induced by shCUL5-CD19 CAR gene transfer into CD8 + T cells from healthy donors. **c** CUL5 to β-actin expression ratio in shGFP- and shCUL5-CD19 CAR T cells. Data are presented from three independent experiments on three different donors. **d**–**f** The expression of unphosphorylated and phosphorylated Janus kinase/signal transducers and activators of transcription (JAK-STAT) proteins was estimated in activated shGFP- and shCUL5-CD19 CAR T cells. The activated cells were harvested four days after co-culturing in a 1:5 E: T ratio with γ-irradiated Raji cells. The JAK/STAT protein to β-actin expression ratio in activated shGFP- and shCUL5-CD19 CAR T cells is shown in (**e**) and (**f**). Data are presented from three independent experiments on three different donors. **g**, **h** JAK1, phospho-JAK1 (p-JAK1), JAK3, and p-JAK3 expressions in wild type (WT)-KHYG-1 and shCUL5-KHYG-1 cells. KHYG-1 cells were stimulated with IL-2 (200 IU/ml) after overnight IL-2 deprivation (**g**). In addition to IL-2 administration, CHX was added at a concentration of 40 μg/ml for the indicated times (**h**). **i** Data on CUL5 and CUL5-related adapter protein KO-CD8 + T cells over time. Cells were prepared in the same manner as CUL5 KO cells from primary human CD8 + T cells and stimulated with anti-CD3/CD28 beads every 10 days. ($n = 5$, different donors) Fig. 5g and h are from one experiment representative of three independent experiments. Data were expressed as mean ± SEM. Statistical significance was determined using the two-sided Student's *t*-test for **c** and the two-way ANOVA with the Šidák multiple comparisons test was used for (**e**, **f**, and **i**. Source data are provided as a Source Data file.

KD-CD19 CAR T cells was greater than that of shGFP-CD19 CAR T cells (Fig. 6f). To analyze the in vivo efficacy of CUL5 KD-CD19 CAR T cells, a subcutaneously injected mouse model was adopted. Because subcutaneously injected tumors better mimic solid tumors and are presumed to be more severe conditions for CD19 CAR T cells, CUL5 KD-CD19 CAR T cells were evaluated in this setting. In the in vivo trials with CUL5 KD-CD19 CAR T cells, CD8+ cell-derived CUL5 KD-CAR T cells were used, and a significantly lower tumor volume (Fig. 6g) and better survival in CUL5 KD-CD19 CAR T cell-treated mice were observed (Fig. 6h). When we compared CUL5 KO- and CUL5 KD-CD19CAR T cells directly in the same Raji iv model, we found that CUL5 KO-CD19 CAR T cells showed significantly superior antitumor effects (Fig. 6i).

Altogether, we suggest that CUL5 downregulation not only improves CAR T cell proliferation in vitro but also enhances CAR T cell therapy efficacy in vivo, and these findings would encourage the use of CAR T cell therapy utilizing the same manufacturing technique adopted in the clinic.

Discussion

GW CRISPR screening system is a powerful tool to identify genes of interest by a large-scale knock out screening. Initially, this system was utilized on cell lines to validate the biomechanical characteristics of cancer cells[38]. Recently, in vivo CRISPR screening with T cells from Cas9 transgenic mice has been employed[39]. Moreover, various investigations indicated successful screening using human primary T cells[15–18]. However, only a few studies performed GW CRISPR screening on human CAR T cells and identified genes of interest[40,41]. In the current study, we hypothesized that human CAR T cell screening could be carried out to identify genes involved in activated human CAR T cell proliferation under tumor Ag stimulation since cell lines and primary T cells have quite distinguished properties based on proliferative signals. To elucidate important mechanisms in the regulation of T cell proliferation, repeated stimulation of CAR T cells with antigen seemed to be an ideal model to analyze T cells in an antigen-specific stimulation mode. Consequently, CUL5 has been identified as a candidate proliferation regulator gene in CD19 CAR T cells employing the

https://doi.org/10.1038/s41467-024-54794-x

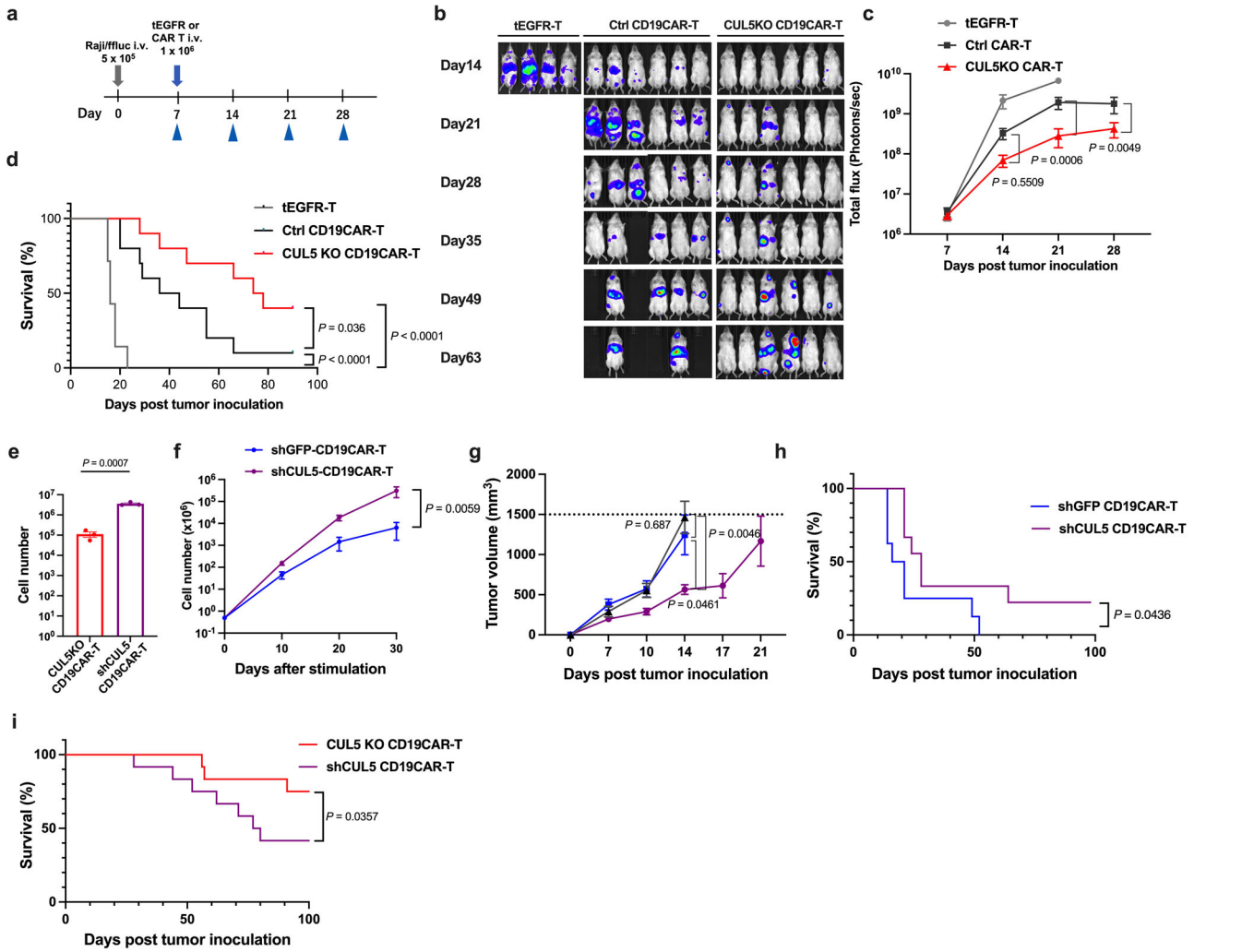

Fig. 6 | In vivo efficacy of CUL5 knockout (KO)- and knockdown (KD)-CD19 CAR T cells. a A schematic diagram of in vivo experiments. Nonobese diabetic/severe combined immunodeficiency (NOD/SCID) common-gamma chain KO (NOG) mice were injected with 5×10^5 Raji/ffluc-green fluorescent protein (GFP) cells via the tail vein on Day 0, followed by 1×10^6 truncated epidermal growth factor receptor (tEGFR)-, control (Ctrl)-, or CUL5 KO-CD19 CAR T cells on Day 7. Tumor burden was assessed using BLI at the indicated time points and weekly thereafter. **b** Representative BLI of Raji-inoculated mice treated with Ctrl- or CUL5 KO-CD19 CAR T cells over time. **c** Tumor burden in mice treated with Ctrl- or CUL5 KO-CD19 CAR T cells at the indicated time points. Data are presented as the mean and SEM, compared using the two-way ANOVA, and acquired from three independent experiments on three different donors (tEGFR-T cells: $n = 4$; Ctrl- and CUL5 KO-CD19 CAR T cells: $n = 9$ per group). **d** Kaplan-Meier survival analysis of Raji/ffluc-bearing NOG mice (log-rank test). **e** The number of CAR T cells derived from 1×10^6 CD8 + T cells on Day 7. Data are derived from three independent experiments on three different donors. Data were expressed as mean ± SEM. **f** The effect of CUL5 KD on activated CD19 CAR T cell proliferation. These cells were stimulated with γ-irradiated Raji cells in a 1:5 E: T ratio every 10 days. Data were expressed as mean ± SEM. ($n = 3$, different donors) Note that the paired *t*-test was used for **e**, whereas the one-way ANOVA was used for (**f**). **g**, **h** In vivo efficacy assessment using a subcutaneous tumor model. On Day 0, Raji/ffluc-GFP cells were subcutaneously inoculated. On Day 10, 1×10^6 tEGFR-, shGFP-, or shCUL5-CD19 CAR T cells were injected. **g** Subcutaneous tumor volume. The curve was censored when any of the mice in the group were euthanized. Data are presented as the mean and SEM, compared using the two-way ANOVA, and acquired from three independent experiments on three different donors ($n = 9$ per group). **h** Kaplan-Meier analysis of NOG mice subcutaneously injected with Raji/ffluc cells (log-rank test). (**i**) Kaplan-Meier analysis of NOG mice intravenously injected with Raji/ffluc cells as in (**a**). 1×10^6 tEGFR-T, CUL5 KO-, or shCUL5-CD19 CAR T cells were injected. Data are acquired from three independent experiments on four different donors (tEGFR-T cells: $n = 8$; CUL5 KO- and shCUL5-CD19 CAR T cells: $n = 12$ per group) (log-rank test). Source data are provided as a Source Data file.

GW CRISPR screening system. We could not assess the effect of CUL5 KO on T cell lines such as Jurkat or SUP-T1 cells, because cell lines grew autonomously. The key to success in GW CRISPR screening in primary human T cells is to ensure that the sgRNA library is adequately covered across the cell population[42]. To solve this issue, a significant number of CD8 + T cells (10–20 million) were transduced with the lentivirus library on Day 1, enabling the detection of almost all sgRNAs in the library from the start. Nonetheless, there was a considerable variation in screening outcomes among individual donors, possibly due to the use of human primary cells. Hence, we determined the *CUL5* gene using GFOLD examination rather than conventional statistical analysis for CRISPR screening[26]. This could be a useful strategy for screening with relatively few biological replicates.

Since our experiments used three different donors and the phenotype of T cells highly differ between donors in terms of phenotype such as CD4/CD8 ratio or naive/ memory phenotype and cell senescence state associated and not associated with donor age, we have not done correlation analysis among experiments. In fact, we identified 6431 guides with GFOLD > 2 between Day 10 and 40, and a total of 777 genes carried 2 or more guides with GFOLD > 2. Among the 777 genes, 6 genes carried 4 guides. The false discovery rate of the 6 genes was < 0.25 based on the null hypothesis that the 6431 guides distributed

randomly to the ~20,000 target genes, suggesting that there should be true hits in top-ranked genes. We have not done a precision-recall analysis of known essential genes also because of the heterogeneity of experiments and a small number of experiments; however, at the very least, guides of known essential genes showed lower abundance and penetration. Because the variation is relatively large in experiments using human cells, heterogeneity among donors was also observed in our experiment. However, T cell proliferation was always better if we applied CUL5 KO or KD and repeated stimulation.

To investigate CUL5 KO-CD19 CAR T cell function, cytokine production capacity was determined, which is a significant indicator of CAR T cell effector functions[8,43]. Remarkably, CUL5 KO elevated cytokine production and shifted the CAR T cell phenotype into the effector memory subset. Because exogenous IL-2 was supplied in our in vitro experiments and we observed increased expression of IL-2 receptor alpha after Ag stimulation, the effect of CUL5 KO may be partly due to the upregulation of IL-2 receptor alpha. CAR T cells with a stem-cell memory phenotype have recently been shown to be less likely to deplete and to have potent antitumor effects[44,45]. CUL5 KO-CD19 CAR T cells preferentially exhibited an effector memory phenotype. Still, their proliferative potential did not reduce even after repeated Ag stimulation, and they demonstrated superior antitumor effects in vivo. In T cells with potentially weak effector function, such as GD2-targeting CAR T cells, CUL5 downregulation could be used to improve effector functionality[7].

CUL5 is a cullin family protein that functions as a scaffold in active cullin-RING ubiquitin ligase complexes[28,31,46,47]. CUL5 maintains cell growth and proliferation, as well as various physiological processes[28]. Its role has been shown primarily across cell line studies. Nevertheless, its role in murine CD4 + T lymphocytes has been identified, but its role in human CD8 + T cells was unknown[48]. Prior research has shown that CUL5 can bind to several adapter proteins and degrade substrates[31,46]. Therefore, we first used RNA-Seq analysis to determine which pathways are primarily modified by CUL5 KO. In addition, CUL5 KO upregulated the expression of several cytokine-related genes, and the JAK/STAT pathway was determined as a top hit in over-representation analysis. Because CUL5 is involved in protein degradation, we investigated the expression of phosphorylated proteins in the JAK/STAT pathway. The findings demonstrated that CUL5 KO enhanced p-STAT3 and p-STAT5 signaling, which is in line with the RNA-Seq analysis findings. It was only in the later stages of culture that a clear increase in T cell proliferation was observed with CUL5 ablation. This may be due to the fact that we observed prolonged phosphorylation of JAK/STAT pathway proteins by CUL5 ablation.

The JAK family includes four tyrosine kinases: JAK1, JAK2, JAK3, and TYK2[49]. They are rapidly stimulated when a specific cytokine or hormone binds to their receptors, and their kinase activities are induced to phosphorylate various effectors and activate downstream signaling pathways. JAK1 and JAK3 are located primarily downstream of IL-2 receptors. Since improved STAT3 and STAT5 signals were observed in CAR T cells cultured with IL-2 supplementation, JAK1, and JAK3 expressions were estimated, and improved p-JAK1 and p-JAK3 expressions were observed in activated CAR T cells. Notably, non-phosphorylated JAK3 was only upregulated upon activation. CUL5 has been shown to form ubiquitin E3 ligase complexes with various adapter proteins to degrade the JAK family[31,47,50]. Still, it is uncertain how CUL5 downregulation affects JAK expression. Thus, we hypothesized that CUL5 KO inhibits JAK3 degradation, specifically in activated cells with enhanced ubiquitin E3 ligase function. Because it is challenging to estimate downstream signaling of IL-2 receptors in primary cells based on reproducibility, the KHYG-1 cell line, an IL-2-dependent tumor cell line, was used to examine the effect of CUL5 KD. Similarly to CAR T cells, p-JAK1 and p-JAK3 expressions were upregulated in CUL5 KD-KHYG-1 cells after IL−2 stimulation, as was JAK3 expression only upon stimulation. JAK1 and JAK3 degradation were delayed by cycloheximide, a protein synthesis inhibitor. Since the interaction between CUL5 and JAKs is mediated by adapter proteins, it could not be analyzed using immunoprecipitation. However, prior research demonstrating JAK binding to adapter proteins associated with CUL5[51] and our findings suggest that CUL5 participated in JAK3 degradation, and thus CUL5 downregulation inhibits JAK3 degradation while enhancing the JAK/STAT pathway. However, we could not show clear and direct evidence supporting that CUL5 ubiquitylates JAK or STAT proteins in our experiments. Our results further suggested that SOCS1, ASB2, and CISH are important substrate receptors associated with CRL5 complex, and that phosphorylated proteins are mainly regulated because the changes in phosphorylated proteins were larger than those in native proteins. We confirmed the KO efficiency for SOCS1, SOCS3, and ASB2, whereas CISH expression could not be confirmed in the T cell line (SUP-T1), but was confirmed in the NK cell line (NK-92). This suggests that the reason why CISH KO was not effective in T cells was due to weak expression in T cells.

A possible reason for the inferior efficacy of shCUL5 CAR T cells could be the lack of IL-2 supply. Although we used CD8+ cells alone in the present study, it is known that CD8+ cells lose their ability to produce IL−2 early after repeated antigen stimulations[52]. Downregulation of CUL5 would enhance downstream signaling of common gamma chain receptors, including IL-2. However, the effect would not be achieved without cytokines. CUL5 KO requires electroporation, resulting in a temporary arrest of cell proliferation, and IL-2 production may be less exhausted. In contrast, during CUL5 KD cell production, cells proliferated well throughout, possibly leading to an early loss of IL-2 production. To investigate this, further studies with cells containing CD4+ cells as a source of IL-2 are warranted.

Our results raised several concerns about the ablation of CUL5. The increased cytokine production causes a concern that cytokine release syndrome may be exacerbated when CUL5 KO CAR T cells applied clinically. It may be a good idea to consider using CUL5 KO in combination with 4-1BB intracellular domain CAR constructs, which induce less cytokine release syndrome[53]. There are also concerns about the feasibility of clinical application of CUL5 KO. Because CRISPR Cas9 genome editing is known to cause problems such as chromosome loss[54], we believe that KD by shRNA is preferable for future clinical applications.

In conclusion, we suggest that CUL5 KO improves expansion potential and effector functions in CD19 CAR T cells via the JAK/STAT pathway. Moreover, genetic modification by targeting CUL5 boosted CD19 CAR T cell treatment outcomes in tumor-bearing mice. These novel findings could aid the launch of important clinical trials and pave the way to improving immunotherapy by regulating the ubiquitin system.

Methods

Human samples

The Institutional Review Board of Nagoya University Graduate School of Medicine approved the research protocols (approval numbers: 2014-0081 and 2017-0445). Peripheral blood mononuclear cells were collected from healthy volunteer donors. Written informed consent was acquired from each donor following the Helsinki Declaration.

Cell lines

Lenti-X 293 T, Phoenix-Ampho, K562, Raji, Jurkat, KHYG-1, and SUP-T1 cell lines were maintained in our laboratory. The authenticity of all cell lines was routinely confirmed by analyzing their immunophenotypes using flow cytometry. Cells were cultured for up to two months prior to use. All cell lines were regularly evaluated with the MycoAlert detection kit (Lonza, LT07-118) to ensure they were not contaminated with mycoplasma. Adherent cell lines were cultured in Dulbecco's Modified Eagle Medium containing 10% fetal bovine serum and 1% penicillin/streptomycin. Cell line suspensions were cultured in Roswell

Park Memorial Institute Medium 1640 containing 10% fetal bovine serum, L-glutamine (0.8 mM), and 1% penicillin/streptomycin. Raji cells were lentivirally transduced with the GFP-firefly luciferase gene and sorted to a purity of greater than 99%. Jurkat TPR cells were transduced with a lentivirus carrying Cas9 and sgRNA targeting CUL5 to create CUL5 KO-Jurkat TPR cells[35]. KHYG-1 cells were transduced with lentivirus carrying shRNA targeting GFP and CUL5 to create GFP KD- and CUL5 KD-KHYG-1 cells. Transduced cells were then chosen using puromycin for 3–6 days.

Lentiviral vector production

For the GW CRISPR screening, the Human GeCKO v2 GW library (Addgene, #1000000048) was used. Lentiviral vector plasmids carrying sgRNA targeting each specified gene as well as eGFP were obtained from VectorBuilder (Chicago, IL, USA). The lentiviral vector plasmid, along with the packaging plasmid psPAX2 and the envelope plasmid pMD2.G, was co-transfected into Lenti-X 293 T using lipofectamine 2000 (Invitrogen, #11668019). The constructed viral vector was harvested 48 hours after transfection and employed immediately for experiments, or it was concentrated by ultracentrifuging the viral supernatant at 24 and 48 hours after transfection and stored at −80 °C for subsequent experiments. Vector IDs are summarized in the Supplementary Table 1 and can be employed to obtain detailed information concerning the vector on vectorbuilder.com.

CD19 CAR retroviral vector construction

CD19 CAR, which includes CD28 (CD28z), was developed by fusing the costimulatory domain with an anti-CD19 single-chain variable fragment-short hinge (12 aa)-CD28 transmembrane domain, followed by the CD3ζ intracellular domain[10]. The CD19 single-chain variable fragment was in line with the clone FMC63 for all CAR constructs in this study[10,43]. CD19 CAR constructs were then fused with a tEGFR lacking EGF binding and intracellular signaling domains downstream of the self-cleaving T2A sequence. tEGFR is employed as a transduction and selection marker by biotinylated Erbitux monoclonal antibody (mAb; Bristol-Myers Squibb)[55–57]. The CAR constructs were then subcloned into the LZRS-pBMN-Z vector, and the sequence was validated by direct sequencing. Gamma retroviral supernatants were developed employing the Phoenix-Ampho system (Orbigen, San Diego, CA, USA). The sequences of the second-generation CAR T cells used in this study were identical to those previously noted and clinically applied[58,59].

Generation and expansion culture of GW CRISPR KO-CD19 CAR T cells and specific genes KO-CD19 CAR T cells

Peripheral blood mononuclear cells were isolated from healthy donors by centrifuging whole blood with Ficoll-Hypaque solution (GE Healthcare, #17144003). $CD8^+$ lymphocytes were then purified with immunomagnetic beads (Miltenyi, #130-045-201) and stimulated with anti-CD3/CD28 beads (Invitrogen, #11141D). On Day 1, GW gRNA-encoding lentiviral particles made from the Human GeCKO v2 library (Addgene #1000000048) were transduced at a multiplicity of infection of 1, and the next day, Cas9 protein (Takara Bio, #632641) was electroporated in a Nucleofector device utilizing the Human T Cell Nucleofector Kit (Lonza, #VPA-1002) following the manufacturer's instructions. On Day 3, CD19 CAR T cells were retrovirally transduced using recombinant human retronectin-coated plates (RetroNectin, Takara Bio, #T100A) preloaded with CD19 CAR-encoding retrovirus and centrifuged at 887 g for two hours at 32 °C. The transduced T cells were then expanded in Roswell Park Memorial Institute Medium 1640 supplemented with 10% human serum, L-glutamine (0.8 mM), 1% penicillin/streptomycin, and 2-mercaptoethanol (0.5 μM), as well as recombinant human IL−2 (50 IU/mL, PeproTech, #200-02). To create specific gene KO-CD19 CAR T cells, gRNA-encoding lentiviral particles targeting specific genes were transduced rather than GW gRNA-encoding lentiviral particles on Day 1. On Day 7, CAR-positive T cells were enriched using biotin-conjugated anti-EGFR mAb and streptavidin beads (Myltenyi, #130-048-101). On Days 10, 20, and 30, the enriched CAR-positive cells were stimulated by co-culture with γ-irradiated Raji at a 1:5 responder to stimulator ratio, with IL-2 supplementation (50 IU/mL) every three days[60]. Because stimulator cells were γ-irradiated in most experiments, those cells would usually disappear within a couple of days. For mice experiments, the enriched CAR-positive cells were induced a second time with anti-CD3/CD28 beads at a 1:3 cell to beads ratio for 7–10 days before use. Control CAR T cells were cultured in the same way as sgRNA-transfected CAR T cells, with the exception of the inclusion of control gRNA-encoding lentivirus.

sgRNA screening of repeatedly stimulated CD19 CAR T cells

On Days 10 and 40, gDNA was extracted from sgRNA-transfected CAR T cells using the QIAamp DNA Blood Mini Kit (Qiagen, #51104). Each gDNA sample had two rounds of polymerase chain reaction (PCR) to increase gRNA cassettes with Illumina sequencing adapters and indexes[16,24]. In the first PCR round, 25 cycles of amplification were carried out employing PrimeSTAR GXL DNA Polymerase (Takara Bio, #R050A). gDNA (16–30 μg) from a given sample was distributed into 16–30 100 μL reaction tubes. A total of 124 reactions were conducted to achieve 150x coverage of the library. Following the first PCR, all PCR products from a given sample were pooled and thoroughly mixed. In the second PCR round, 5 μL of the first-round PCR product was applied as a template in each 100 μL reaction. Each sample had six amplification cycles to include each index sequence. The second PCR product from a given sample was pooled and purified with AMPure XP beads (catalog no. A63381; Beckman Colter, #A63381) at a DNA: beads ratio of 1:1.8 following the manufacturer's instructions. After being eluted with 50 μL of nuclease-free water, all DNA libraries were checked using Agilent 2200 TapeStation and D1000 ScreenTape (Agilent, #5067-5584). DNA concentrations were also measured using the Qubit dsDNA HS assay kit (Thermo Fisher Scientific, #Q32854). All samples were pooled and sequenced on an Illumina HiSeq X with 2 × 150 bp end-reads to acquire 20–30 million reads per sample. Reads Per Kilobase of the transcript, per Million mapped reads (RPKM) were computed using GFOLD[26]. Alterations in expression levels between groups were estimated using GFOLD, and the resulting GFOLD (0.1) values (conservative estimation of fold changes at the confidence level (q) of 0.1) were used to identify candidate genes.

Flow cytometry and immunophenotyping

All samples were examined using flow cytometry on a FACSAria II and LSR Fortessa (BD Biosciences), and the data were evaluated using FlowJo software (Tree Star). The GFP marker was utilized to examine the proliferation of sgRNA-positive CAR T cells and T cells. Human T cells were stained with combinations of the following mAb conjugated to fluorophores: CD8 (clone RPA-T8); CD45RA (clone HI100); CCR7 (clone 150503); IL-2 (clone 5344.111); interferon-gamma (IFN-γ, clone 25723.11); programmed cell death 1 (clone EH12.1); lymphocyte-activation gene 3 (clone T47-530) (All BD Biosciences); cytotoxic T-lymphocyte-associated protein 4 (clone L3D10); and T-cell immunoglobulin mucin-3 (clone F38-2E2) (BioLegend). $tEGFR^+$ cells were identified using biotinylated Erbitux and streptavidin-Phycoerythrin (BD Biosciences, #554061).

Proliferation assay

To examine activated CD19 CAR T cell and CD37 CAR T cell proliferation, CAR T cells were activated with γ-irradiated Raji at a 1:5 responder to stimulator ratio on Days 10, 20, and 30, with 50 IU/mL IL-2 supplementation every three days. The activated CD8 + T cells were induced with anti-CD3/CD28 beads. CTV (Invitrogen, # C34557), Ki67 (BioLegend, #350513), and EdU reagents (Invitrogen, #C10634) were utilized for proliferation assays in line with the manufacturer's protocol.

Cytotoxicity and apoptosis assay

To differentiate apoptotic cells derived from CAR T cells and Raji cells, Raji cells were stained with CTV. CAR T cells were co-cultured with Raji cells in the suggested ratio and then stained using the APC Annexin V apoptosis detection kit with propidium iodide (BioLegend, #640932) following the manufacturer's protocol at the time indicated post-stimulation.

Intracellular cytokine staining and cytokine secretion assay

Control CD19 CAR T cells and CUL5 KO-CD19 CAR T cells were plated at a 1:2 E: T ratio with either K562 or Raji cells along with brefeldin A (Sigma-Aldrich, #B7651) for four hours. To detect intracellular cytokines, the stimulated cells were fixed and permeabilized using a Cell Fixation/Permeabilization Kit (BD Biosciences, #554714) and then stained with anti-IL-2 or anti-IFN-γ mAbs.

RNA-Seq analysis

Control sgRNA-transduced CD19 CAR T cells and CUL5 sgRNA-transduced CD19 CAR T cells were induced with γ-irradiated Raji cells at a 1:5 E: T ratio and the gRNA-positive fraction was sorted by FACSAria II on Day 8 post-stimulation. Total RNA was isolated and purified from their cells using the QIAamp RNA Blood Mini Kit (Qiagen, #52304). RNA-Seq libraries were prepared employing the NEBNext Ultra II RNA Library Prep Kit for Illumina (New England Biolabs, #E7770) and the NEBNext Poly(A) mRNA Magnetic Isolation Module (New England Biolabs, #E7490) following the manufacturer's instructions and sequenced on an Illumina HiSeqX with 2 × 150 base paired-end reads. First, the raw read data quality was assessed for each sample using FastQC (Version 0.11.9) for RNA-Seq analysis. Transcript abundances were then directly quantified from the raw RNA-Seq FASTQ files using the Kallisto v0.44.0 pseudoalignment method[61]. For rapid and accurate quantification, a transcriptome index constructedbuilt from the Ensembl project's transcriptome v91 with a 100 bootstrap value based on the pseudoalignment was used. Gene-by-gene expression matrices were created using the R package tximport. Consequently, differential expression was analyzed using an integrated web application for differential expression and pathway analysis of RNA-Seq data (iDEP)[62]. Functional analyzes like enrichment and pathway analyzes were conducted using Metascape (http://metascape.org/) and WebGestalt[63,64].

Intracellular phosphoflow analysis

CAR T cells or tEGFR+ T cells were mixed with γ-irradiated Raji cells in a 1:5 ratio, spun down briefly, and incubated at 37 °C for the indicated times for p-p38, p-Erk, p-STAT3, and p-STAT5. Cells were then fixed in 2% formaldehyde at 37 °C for 10 minutes, permeabilized in ice-cold 90% methanol, and placed on ice for 30 minutes. For staining, the following phospho-specific Abs were employed: p38 (pT180/pY182, clone D3F9, #4511), Erk1/2 (pT202/pY204, clone D13.14.4E, #4370), p-STAT3 (pY705, clone D3A7, #9145), and p-STAT5 (pY694, clone D47E7, #4322; all unconjugated; Cell Signaling Technology [CST]), in addition to donkey anti-rabbit IgG-Alexa Fluor 647 (secondary Ab; Invitrogen, #A-31573).

Jurkat TPR cell line assay

To assess NF-κB, AP-1 and NFAT signal transduction, we used the Jurkat-TPR cells that contains response elements for NF-κB, AP-1 and NFAT, which drive the expression of the fluorescent proteins cyan fluorescent protein, mCherry and enhanced green fluorescent protein (eGFP), respectively[35,36]. Wild type Jurkat TPR cells and CUL5-KO Jurkat TPR cells were retrovirally transduced with CD19CAR. CAR-positive cells were enriched using biotin-conjugated anti-EGFR mAb and streptavidin beads (Miltenyi, #130-048-101). Jurkat-TPR cells were harvested and analyzed for expression of the fluorescent protein of interest using flow cytometry.

Immunoblotting

Cells were washed in cold phosphate-buffered saline after harvesting and lysed in 1x lysis buffer (R&D Systems, #895561) with 1x protease inhibitor cocktail (Sigma-Aldrich, #P8340). Lysates were incubated on ice for 15 minutes and cleared by centrifugation at 11,700 × *g* for 15 minutes. Protein concentrations were determined using the Quick Start™ of Bradford 1x Dye Reagent (Bio-Rad, #5000205JA). Total protein (20 μg) was mixed with a sample buffer comprising 5% 2-mercaptoethanol and denatured at 95 °C for five minutes. The samples were separated using sodium dodecyl-sulfate polyacrylamide gel electrophoresis and transferred to a polyvinylidene fluoride membrane (Millipore, #IPVH00010). Membranes were blocked with 5% (w/v) nonfat dry milk in Tris-buffered saline Tween buffer (Tris-HCL [50 mM, pH 7.4], NaCl [150 mM], and 0.05% Tween 20) and incubated with primary antibodies overnight at 4 °C and horseradish peroxidase-conjugated secondary antibodies (CST, #7074) for two hours at room temperature. The signal was observed with an ECL™ Prime Western Blotting System (Cytiva, #GERPN2236), visualized with a LAS-4000 mini-image analyzer (FUJIFILM), and analyzed with MultiGauge software (FUJIFILM). Primary antibodies used were rabbit anti-CUL5 (1:1000; Abcam, #ab184177), mouse anti-β-actin (1:2000; Santa Cruz, #sc-271800), anti-JAK1 (1:1000; CST, #3344), anti-JAK2 (1:1000; CST, #3230), anti-JAK3 (1:1000; CST, #8827), anti-TYK2 (1:1000; CST, #14193), anti-p-JAK1 (1:1000; CST, #74129), anti-p-JAK2 (1:1000; CST, #8082), anti-p-JAK3 (1:1000; CST, #5031), anti-p-TYK2 (1:1000; CST, #68790), anti-STAT3 (1:1000; CST, #4904), anti-STAT5 (1:1000; CST, #94205), anti-SOCS1 (1:1000; CST, #68631), anti-SOCS3 (1:2000; proteintech, #14025-1-AP), anti-ASB2 (1:1000; antibodies.com, #A90859), anti-CISH (1:1000; CST, #8731).

To validate KO efficiency of substrate receptor, we transfected the respective sgRNAs into SUP-T1 or NK-92 cell lines, electroporated the Cas9 protein, and performed western blotting.

Lentiviral two-in-one vector plasmid construction

The annealed shRNA oligonucleotides targeting GFP and CUL5 were inserted between the restriction sites in the pGreenPuro shRNA vector (SBI, #SI506A-1). Subsequently, the sequence EF1-copGFP-T2A-puro was replaced with the sequence EF-1α-CD19CAR-T2A-tEGFR, and the inserted DNA sequences of each vector were validated by direct DNA sequencing. The shRNA sequence targeting GFP was GCA-GACTGAATTAGTAGAAAT, while shRNA sequences targeting human CUL5 were GCTAGAATGTTTCAGGACATA (shCUL5#1) and GCAAGCTGACCCTGAAGTTCAT (shCUL5#2). We adopted shCUL5#2 to create shCUL5-CD19 CAR T cells.

Raji xenograft model and bioluminescence imaging (BLI)

The Institutional Animal Care and Use Committee of Nagoya University Graduate School of Medicine approved all murine experimental protocols. All mice were maintained at the Division of Experimental Animals in specific pathogen-free/SPF conditions. Six to seven-week-old male NOD/Shi-scid, IL−2RγKO Jic (NOG) mice (In-Vivo Science) were intravenously inoculated with 0.5×10^6 Raji-ffluc cells via the tail vein. One week later, they were treated with tEGFR-, control-, or CUL5 KO-CD19 CAR T cells (intravenous model). In addition, six to seven-week-old male NOG mice were subcutaneously inoculated with 2.0×10^6 Raji-ffluc cells. Ten days later, they were treated with tEGFR-transduced T cells, shGFP-CD19 CAR T cells, or shCUL5-CD19 CAR T cells (subcutaneous model). At the indicated time points, tumor progression was assessed with BLI using the IVIS Spectrum System (Caliper Life Science, IVIS Lumina III). In the subcutaneous model, tumors were measured twice a week from Day 14 after tumor injection until death. Death was determined when a progressively growing tumor reached 2.0 cm in the longest dimension. The longest dimension (length) and the longest perpendicular dimension (width) were manually measured. Tumor volume was calculated using the following formula:

$(L \times W^2)/2$. In the survival analysis, death was used as an endpoint. Mice were euthanized by inhalation of carbon dioxide when necessary.

Statistical analysis

All experimental data are denoted as the mean and standard error of the mean or standard deviation. The Student's *t*-test and one-way or two-way analysis of variance (ANOVA) with Bonferroni's or Tukey's post-test correction were used to determine differences between results, as suitable. The Kaplan-Meier method with the log-rank test was used to compare survival times. A *p*-value of less than 0.05 was considered statistically significant. GraphPad Prism Version 9.3.1 software (GraphPad Software) was used for statistical analysis.

Reporting summary

Further information on research design is available in the Nature Portfolio Reporting Summary linked to this article.

Data availability

Raw sequencing data obtained in this study were deposited to the Sequence Read Archive underthe NCBI BioProject accession no. PRJDB17246. All data are included in the Supplementary Information or available from the authors, as are unique reagents used in this Article. The raw numbers for charts and graphs are available in the Source Data file. Source data are provided with this paper.

References

1. Abramson, J. S. et al. Lisocabtagene maraleucel for patients with relapsed or refractory large B-cell lymphomas (TRANSCEND NHL 001): a multicentre seamless design study. *Lancet* **396**, 839–852 (2020).
2. Schuster, S. J. et al. Tisagenlecleucel in adult relapsed or refractory diffuse large B-cell lymphoma. *N. Engl. J. Med* **380**, 45–56 (2019).
3. Neelapu, S. S. et al. Axicabtagene ciloleucel CAR T-cell therapy in refractory large B-cell lymphoma. *N. Engl. J. Med*. **377**, 2531–2544 (2017).
4. Grupp, S. A. et al. Chimeric antigen receptor-modified T cells for acute lymphoid leukemia. *N. Engl. J. Med* **368**, 1509–1518 (2013).
5. Chen, G. M. et al. Integrative bulk and single-cell profiling of premanufacture T-cell populations reveals factors mediating long-term persistence of CAR T-cell therapy. *Cancer Discov.* **11**, 2186–2199 (2021).
6. Turtle, C. J. et al. CD19 CAR–T cells of defined CD4+:CD8+ composition in adult B cell ALL patients. *J. Clin. Investig.* **126**, 2123–2138 (2016).
7. Lynn, R. C. et al. c-Jun overexpression in CAR T cells induces exhaustion resistance. *Nature* **576**, 293–300 (2019).
8. Guedan, S. et al. Single residue in CD28-costimulated CAR-T cells limits long-term persistence and antitumor durability. *J. Clin. Investig.* **130**, 3087–3097 (2020).
9. Zhao, Z. et al. Structural design of engineered costimulation determines tumor rejection kinetics and persistence of CAR T cells. *Cancer cell* **28**, 415–428 (2015).
10. Julamanee, J. et al. (2021) Composite CD79A/CD40 co-stimulatory endodomain enhances CD19CAR-T cell proliferation and survival. *Mol Ther*, **29**, 2677–2690 (2021).
11. Seo, H. et al. BATF and IRF4 cooperate to counter exhaustion in tumor-infiltrating CAR T cells. *Nat. Immunol.* **22**, 983–995 (2021).
12. Wang, Y. et al. Low-dose decitabine priming endows CAR T cells with enhanced and persistent antitumour potential via epigenetic reprogramming. *Nat. Commun.* **12**, 409 (2021).
13. Yoshikawa, T. et al. Genetic ablation of PRDM1 in antitumor T cells enhances therapeutic efficacy of adoptive immunotherapy. *Blood* **139**, 2156–2172 (2022).
14. Ren, J. et al. Multiplex genome editing to generate universal CAR T cells resistant to PD1 inhibition. *Clin. Cancer Res* **23**, 2255–2266 (2017).
15. Parnas, O. et al. A genome-wide CRISPR screen in primary immune cells to dissect regulatory networks. *Cell* **162**, 675–686 (2015).
16. Shalem, O. et al. Genome-scale CRISPR-Cas9 knockout screening in human cells. *Science* **343**, 84–87 (2014).
17. Wang, T., Wei, J. J., Sabatini, D. M. & Lander, E. S. Genetic screens in human cells using the CRISPR-Cas9 system. *Science* **343**, 80–84 (2014).
18. Shifrut, E. et al. Genome-wide CRISPR screens in primary human T cells reveal key regulators of immune function. *Cell* **175**, 1958–1971.e1915 (2018).
19. Gurusamy, D. et al. Multi-phenotype CRISPR-Cas9 screen identifies p38 kinase as a target for adoptive immunotherapies. *Cancer cell* **37**, 818–833.e819 (2020).
20. Patel, S. J. et al. Identification of essential genes for cancer immunotherapy. *Nature* **548**, 537–542 (2017).
21. Sutra Del Galy, A. et al. In vivo genome-wide CRISPR screens identify SOCS1 as intrinsic checkpoint of CD4(+) T(H)1 cell response. *Sci. Immunol.* **6**, eabe8219 (2021).
22. Loo, C. S. et al. A genome-wide CRISPR screen reveals a role for the non-canonical nucleosome-remodeling BAF complex in Foxp3 expression and regulatory T cell function. *Immunity* **53**, 143–157.e148 (2020).
23. Yin, H., Xue, W. & Anderson, D. G. CRISPR-Cas: a tool for cancer research and therapeutics. *Nat. Rev. Clin. Oncol.* **16**, 281–295 (2019).
24. Sanjana, N. E., Shalem, O. & Zhang, F. Improved vectors and genome-wide libraries for CRISPR screening. *Nat. Methods* **11**, 783–784 (2014).
25. Heo, S. J. et al. Compact CRISPR genetic screens enabled by improved guide RNA library cloning. *Genome Biol.* **25**, 25 (2024).
26. Feng, J. et al. GFOLD: a generalized fold change for ranking differentially expressed genes from RNA-seq data. *Bioinformatics* **28**, 2782–2788 (2012).
27. Okuno, S. et al. Spacer length modification facilitates discrimination between normal and neoplastic cells and provides clinically relevant CD37 CAR T cells. *J. Immunol.* **206**, 2862–2874 (2021).
28. Zhao, Y., Xiong, X. & Sun, Y. Cullin-RING ligase 5: functional characterization and its role in human cancers. *Semin Cancer Biol.* **67**, 61–79 (2020).
29. Ilangumaran, S., Bobbala, D. & Ramanathan, S. SOCS1: regulator of T cells in autoimmunity and cancer. *Curr. Top. Microbiol Immunol.* **410**, 159–189 (2017).
30. Yoshimura, A., Ito, M., Chikuma, S., Akanuma, T. & Nakatsukasa, H. Negative regulation of cytokine signaling in immunity. *Cold Spring Harb. Perspect. Biol.* **10**, a028571. (2018).
31. Okumura, F., Joo-Okumura, A., Nakatsukasa, K. & Kamura, T. The role of cullin 5-containing ubiquitin ligases. *Cell Div.* **11**, 1 (2016).
32. Rochman, Y., Spolski, R. & Leonard, W. J. New insights into the regulation of T cells by γc family cytokines. *Nat. Rev. Immunol.* **9**, 480–490 (2009).
33. Leonard, W. J., Lin, J. X. & O'Shea, J. J. The γ(c) family of cytokines: basic biology to therapeutic ramifications. *Immunity* **50**, 832–850 (2019).
34. Kershaw, M. H., Westwood, J. A. & Darcy, P. K. Gene-engineered T cells for cancer therapy. *Nat. Rev. Cancer* **13**, 525–541 (2013).
35. Jutz, S. et al. Assessment of costimulation and coinhibition in a triple parameter T cell reporter line: Simultaneous measurement of NF-kappaB, NFAT and AP-1. *J. Immunol. Methods* **430**, 10–20 (2016).
36. Rydzek, J. et al. Chimeric antigen receptor library screening using a novel NF-κB/NFAT reporter cell platform. *Mol. Ther.* **27**, 287–299 (2019).

37. Zhu, H. et al. Metabolic reprograming via deletion of CISH in human iPSC-derived NK cells promotes in vivo persistence and enhances anti-tumor activity. *Cell Stem Cell* **27**, 224–237.e226 (2020).
38. Chen, S. et al. Genome-wide CRISPR screen in a mouse model of tumor growth and metastasis. *Cell* **160**, 1246–1260 (2015).
39. LaFleur, M. W. et al. A CRISPR-Cas9 delivery system for in vivo screening of genes in the immune system. *Nat. Commun.* **10**, 1668 (2019).
40. Freitas, K. A. et al. Enhanced T cell effector activity by targeting the Mediator kinase module. *Science* **378**, eabn5647 (2022).
41. Wang, D. et al. CRISPR screening of CAR T cells and cancer stem cells reveals critical dependencies for cell-based therapies. *Cancer Discov.* **11**, 1192–1211 (2021).
42. Yau, E. H. & Rana, T. M. Next-generation sequencing of genome-wide CRISPR screens. *Methods Mol. Biol.* **1712**, 203–216 (2018).
43. Kowolik, C. M. et al. CD28 costimulation provided through a CD19-specific chimeric antigen receptor enhances in vivo persistence and antitumor efficacy of adoptively transferred T cells. *Cancer Res* **66**, 10995–11004 (2006).
44. Alizadeh, D. et al. IL15 enhances CAR-T Cell antitumor activity by reducing mTORC1 activity and preserving their stem cell memory phenotype. *Cancer Immunol. Res.* **7**, 759–772 (2019).
45. Arcangeli, S. et al. CAR T cell manufacturing from naive/stem memory T lymphocytes enhances antitumor responses while curtailing cytokine release syndrome. *J. Clin. Invest* **132**, e150807 (2022).
46. Gao, F. et al. The functions and properties of cullin-5, a potential therapeutic target for cancers. *Am. J. Transl. Res* **12**, 618–632 (2020).
47. Petroski, M. D. & Deshaies, R. J. Function and regulation of cullin-RING ubiquitin ligases. *Nat. Rev. Mol. Cell Biol.* **6**, 9–20 (2005).
48. Kumar, B. et al. The ubiquitin ligase Cul5 regulates CD4(+) T cell fate choice and allergic inflammation. *Nat. Commun.* **13**, 2786 (2022).
49. Bharadwaj, U., Kasembeli, M. M., Robinson, P. & Tweardy, D. J. Targeting Janus kinases and signal transducer and activator of transcription 3 to treat inflammation, fibrosis, and cancer: rationale, progress, and caution. *Pharm. Rev.* **72**, 486–526 (2020).
50. Liau, N. P. D. et al. The molecular basis of JAK/STAT inhibition by SOCS1. *Nat. Commun.* **9**, 1558 (2018).
51. Wu, W. & Sun, X. H. A mechanism underlying NOTCH-induced and ubiquitin-mediated JAK3 degradation. *J. Biol. Chem.* **286**, 41153–41162 (2011).
52. Wherry, E. J. & Kurachi, M. Molecular and cellular insights into T cell exhaustion. *Nat. Rev. Immunol.* **15**, 486–499 (2015).
53. Kamdar, M. et al. Lisocabtagene maraleucel versus standard of care with salvage chemotherapy followed by autologous stem cell transplantation as second-line treatment in patients with relapsed or refractory large B-cell lymphoma (TRANSFORM): results from an interim analysis of an open-label, randomised, phase 3 trial. *Lancet* **399**, 2294–2308 (2022).
54. Tsuchida, C. A. et al. Mitigation of chromosome loss in clinical CRISPR-Cas9-engineered T cells. *Cell* **186**, 4567–4582.e4520 (2023).
55. Watanabe, K. et al. Target antigen density governs the efficacy of anti-CD20-CD28-CD3 ζ chimeric antigen receptor-modified effector CD8+ T cells. *J. Immunol.* **194**, 911–920 (2015).
56. Paszkiewicz, P. J. et al. Targeted antibody-mediated depletion of murine CD19 CAR T cells permanently reverses B cell aplasia. *J. Clin. Investig.* **126**, 4262–4272 (2016).
57. Sakemura, R. et al. A Tet-On Inducible System for Controlling CD19-Chimeric Antigen Receptor Expression upon Drug Administration. *Cancer Immunol. Res.* **8**, 658–68 (2016).
58. Hudecek, M. et al. Receptor affinity and extracellular domain modifications affect tumor recognition by ROR1-specific chimeric antigen receptor T cells. *Clin. Cancer Res.* **19**, 3153–3164 (2013).
59. Wang, X. et al. Phase 1 studies of central memory-derived CD19 CAR T-cell therapy following autologous HSCT in patients with B-cell NHL. *Blood* **127**, 2980–2990 (2016).
60. Terakura, S. et al. Generation of CD19-chimeric antigen receptor modified CD8+ T cells derived from virus-specific central memory T cells. *Blood* **119**, 72–82 (2012).
61. Sarantopoulou, D. et al. Comparative evaluation of full-length isoform quantification from RNA-Seq. *BMC Bioinforma.* **22**, 266 (2021).
62. Ge, S. X., Son, E. W. & Yao, R. iDEP: an integrated web application for differential expression and pathway analysis of RNA-Seq data. *BMC Bioinforma.* **19**, 534 (2018).
63. Zhou, Y. et al. Metascape provides a biologist-oriented resource for the analysis of systems-level datasets. *Nat. Commun.* **10**, 1523 (2019).
64. Liao, Y., Wang, J., Jaehnig, E. J., Shi, Z. & Zhang, B. WebGestalt 2019: gene set analysis toolkit with revamped UIs and APIs. *Nucleic Acids Res* **47**, W199–w205 (2019).

Acknowledgements

The authors would like to thank the Division of Experimental Animals and the Division of Medical Research Engineering at Nagoya University Graduate School of Medicine for their technical assistance. This work was supported by grants from the Japan Society for the Promotion of Science (JSPS) KAKENHI (18k08351 and 22k08501 to S.T.), the Practical Research Project for Allergic Diseases and Immunology (19ek0510022h0003 to S.T. and M.M.), and the Japan Science and Technology Agency (JST) CREST (JPMJCR19H4 to Y.S.).

Author contributions

Conception and design: Y.A. and S.T. Data acquisition: Y.A., S.T., M.O., Y.O., Y.S., K.S., Y.T., H.Y., K.I., and R.H. Data analysis and interpretation (e.g., statistical analysis, biostatistics, and computational analysis): Y.A., S.T., Y.O., and Y.S. Manuscript writing, review, and/or revision: Y.A., S.T., Y.O., P.S., M.M., and H.K. Administrative, technical, or material support (e.g., reporting or organizing data and constructing databases): Y.S., P.S., J.L., M.M., and H.K. Study supervision: S.T., M.M., and H.K.

Competing interests

Y. Adachi, S. Terakura, and H. Kiyoi are inventors on patent applications for CUL5 modification technologies submitted by Nagoya University, Nagoya, Japan. H. Kiyoi has received research funding from FUJIFILM, Kyowa-Kirin, Bristol-Myers Squibb, Otsuka, Perseus Proteomics, Daiichi Sankyo, Abbvie, CURED, Astellas Pharma, Chugai, Zenyaku Kogyo, Nippon Shinyaku, Eisai, Takeda, Sumitomo Pharma, and Sanofi, in addition to honoraria from Abbvie, Chugai, Astellas Pharma, and Novartis. The other authors declare no competing financial or non-financial interests.

Additional information

Supplementary information The online version contains supplementary material available at https://doi.org/10.1038/s41467-024-54794-x.

Correspondence and requests for materials should be addressed to Yoshitaka Adachi or Seitaro Terakura.

Peer review information *Nature Communications* thanks Paula Oliver and the other anonymous reviewer(s) for their contribution to the peer review of this work. A peer review file is available.